Analytica Chimica Acta 711 (2012) 40–45

Contents lists available at SciVerse ScienceDirect

Analytica Chimica Acta

journal homepage: www.elsevier.com/locate/aca

A simple and an efficient strategy to synthesize multi-component nanocomposites for biosensor applications

Xiaoquan Lu*, Yan Li, Xia Zhang, Jie Du, Xibin Zhou, Zhonghua Xue, Xiuhui Liu

Key Laboratory of Bioelectrochemistry & Environmental Analysis of Gansu Province, College of Chemistry & Chemical Engineering, Northwest Normal University, Lanzhou 730070, China

ARTICLE INFO

Article history:
Received 20 August 2011
Received in revised form 27 October 2011
Accepted 2 November 2011
Available online 11 November 2011

Keywords:
One-step
Au–polypyrrole (PPy)/Prussian blue (PB)
Multi-component nanocomposites
Biosensor

ABSTRACT

We demonstrate that core–shell multi-component nanocomposites can be grown in situ at room temperature by a novel one-step approach without adding any reductant and stabilizer. We have presented a one-step method for the synthesis of multi-component nanocomposites in water solution, the multi-component nanocomposites could be produced directly and quickly in an in situ wet-chemical reaction. Here, Au–polypyrrole (PPy)/Prussian blue (PB) nanocomposites have been synthesized successfully under the same circumstance. With the addition of pyrrole monomers into mixture solutions, the autopolymerization of pyrrole into PPy and $AuCl_4^-$ was reduced to elemental Au instantaneously as well as simultaneously. At the same time, PB produced along with elemental Au serving as a catalyst. Furthermore, we investigated the performance of Au–PPy/PB nanocomposites as amperometric sensor toward the reduction of H_2O_2, which displayed high sensitivity, fast response and good stability. The peak current of H_2O_2 increased linearly with the concentration of H_2O_2 in the range from 2.5×10^{-9} to 1.2×10^{-6} M, and the low detection limit of 8.3×10^{-10} M (S/N = 3) was obtained. Therefore, this work provides a new pathway to design and fabricate novel multi-component nanocomposites, which have unique characteristics and hold great applications in the fields of sensors, electrocatalysis and others.

1. Introduction

Nanocomposites are considered to be a group of perspective substances, combining together the different properties of components, leading the way to a new, tunable behavior, and the special characteristics of multi-component nanocomposite has received great attention [1]. Various synthesis methods have been developed as their wide applications [2–4], such as chemical reduction [5], sonochemical reduction [6], laser ablation [7], radiolytic reduction [8], metal evaporation [9], and Ar+ ion sputtering [10], etc. These methods have their own advantages but most synthesis procedure of nanocompositises are multiple steps and need presynthesized precursor. Tsai et al. prepared Au–Ag–Pd nanoparticles by laser irradiation [11]. Perruchot et al. investigated polypyrrole-APS-silica particles which APS was first grafted onto the silica particles then pyrrole coating and polymerization [12]. It is much worthy of being found facile ways to get desired nanocomposites such as one-step method. There are some instances employing one-step method to prepare two-component nanocomposites, for example, CdS/montmo-srillonite [13], multiwalled carbonnanotube/gold [14], poly(styrene-b-caprolactone)/silicate [15], gold-poly(o-phenylenediamine) [16], polyacrylamide-calcium phosphate (PAM-CP) [17]. However, little research through one-step method preparation of three- or multi-component nanocomposites have been reported, limiting their applications to a large extent. Therefore, a great challenge is how to synthesize nanocomposites, not only one-step but also containing multi-component to the future materials research.

Prussian blue (PB) is a prototype of mixed valence metal hexacyanoferrates, has played a lot of important roles in the fields of electrocatalysis [18], electroanalysis [19,20], electrochromism [21] and batteries [22,23] for its interesting electrochemical, photophysical, and magnetic properties. Especially in the field of electroanalytical chemistry for constructing PB-based H_2O_2 biosensor, it has proved to be an excellent catalyst for H_2O_2 reduction at low potentials. Among various types of conducting polymers, polypyrrole (PPy) is one of the most important organic conducting polymers because of relatively high conductivity, good environmental stability and ease of preparation [24,25]. It has potential use in fuel cells [26,27], sensors [28–31], batteries [32–34], capacitors [35–37], and corrosion protection [38–40]. Conducting polymers have one distinct advantage that is oxidation polymerization of monomer and reduction of metal salt can be finished in one step [41]. Selvan et al. revealed that Au/PPy core–shell NPs can

* Corresponding author. Tel.: +86 931 7971276; fax: +86 931 7971323.
E-mail address: luxq@nwnu.edu.cn (X. Lu).

0003-2670/$ – see front matter © 2011 Elsevier B.V. All rights reserved.
doi:10.1016/j.aca.2011.11.005

synthesize by a simple one-step progress [42], and the conductivity and the sensing behavior of PPy could be further improved by imbedding Au nanoparticles (AuNPs) into the PPy matrix [42–44]. In addition, integrating AuNPs into PB can improve the sensing properties of PB [45]. In this paper, we have successfully synthesized a new multi-component nanocomposites by a one-step method. The morphology and composition of Au–PPy/PB core–shell nanocomposites were investigated by Transmission electron microscopy (TEM), X-ray diffraction (XRD), Fourier transform infrared spectroscopy (FT-IR), ultraviolet visible spectroscopy (UV–vis) and cyclic voltammetry (CV). Moreover, Au–PPy/PB nanocomposites were immobilized on the GCE and construct a H_2O_2 biosensor. The sensor exhibited high sensitivity, fast response and good stability.

2. Experimental

2.1. Chemicals and apparatus

Pyrrole was purchased from Zhongqin Chemical Reagent Co., Ltd. (Shanghai, China) and purified twice by distillation under the protection of high purity nitrogen and then kept in a refrigerator before use. Potassium ferricyanide was purchased from Xi'an Chemical Reagent Factory (Xi'an, China). Chloroauric acid was purchased from Sinopharm Chemical Reagent Co., Ltd. (Shanghai, China). The 0.02 M phosphate buffer solution (PBS), which was made from K_2HPO_4 and KH_2PO_4, was always employed as the supporting electrolyte. All other chemicals were of analytical-reagent grade and used without further purification. All experiments were carried out at room temperature (22 ± 2 °C) and the solutions were prepared by doubly distilled water.

The morphologies of Au–PPy/PB core–shell nanocomposites were observed by TEM (Tecnai G2 F20 U-TWIN, USA). XRD pattern was performed on D/Max-2400 (X-ray Diffractometer, Rigaku Corporation, Tokyo, Japan), UV–vis absorption spectra of Au–PPy/PB core–shell nanocomposites dispersed in distilled water through ultrasonic irradiation were recorded on a UV1102 (Techcomp Bio-Equipment Ltd., Shanghai, China) spectrometer. FTIR spectroscopic measurements were performed on a Nicolet Impact-400 spectrometer using KBr pressed disks. CV and differential pulse voltammetry (DPV) experiments were performed on CHI-832 working station (CHI instrument, Co. Ltd., Austin, USA). A three-electrode system consisting of a sat. Hg/Hg_2Cl_2:KCl reference electrode, a platinum counter electrode as a auxiliary electrode, and a Au–PPy/PB core–shell nanocomposites modified glassy carbon electrode (GCE, $r = 1.75$ mm) was employed for electrochemical measurements.

2.2. Preparation of Au–PPy/PB core–shell nanocomposites

In a typical procedure for the synthesis of Au–PPy/PB nanocomposite, 0.1 M pyrrole aqueous solution was slowly added to a mixed aqueous solution of 1 mM $HAuCl_4$ and 2.5 mM $K_3[Fe(CN)_6]$ at room temperature under vigorous stirring. With the addition of pyrrole aqueous solution, the color changed from green yellow to green blue. The reaction was allowed to proceed for 2 h at room temperature. After the reaction, the mixture was centrifuged, and the precipitate was washed with distilled water for several times. The final product was dried in a vacuum at 60 °C for 24 h.

2.3. Preparation of Au–PPy/PB core–shell nanocomposites modified GCE

The GCE was polished with 0.3, and 0.05 μm alumina slurry followed by rinsing with doubly distilled water and drying at room temperature. Au–PPy/PB core–shell nanocomposites were dispersed in distilled water to form a 1.0 mg mL^{-1} solution and ultrasonically treated for 30 min. The colloidal solution (5 μL) was dropped onto the pretreated GCE surface and allowed to dry under the ambient condition.

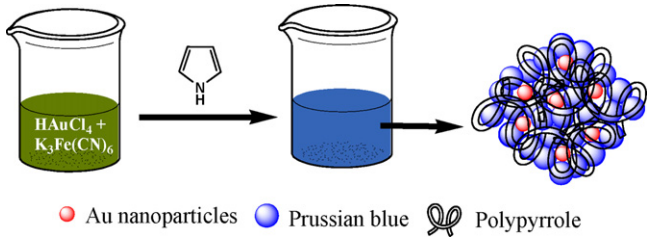

Scheme 1. Synthetic procedure and chemical structure of the Au–PPy/PB core–shell nanocomposites.

3. Results and discussion

3.1. Characterization of Au–PPy/PB core–shell nanocomposites

The synthetic procedure and the chemical structure of the Au–PPy/PB core–shell nanocomposites are shown in Scheme 1. The Au–PPy/PB core–shell nanocomposites were synthesized successfully by one-step with $HAuCl_4$, $K_3[Fe(CN)]_6$ and pyrrole monomer. Fig. 1(a–d) shows the TEM images of the forming Au–PPy/PB core–shell nanocomposites after 0.1 M pyrrole aqueous solution was added to the mixed solution of 1 mM $HAuCl_4$ and 15–25 mM $K_3[Fe(CN)]_6$ solution. As shown in Fig. 1, the dark spots inside the nanocomposites correspond to Au, that is surrounded by PPy/PB matrix. The concentration of $K_3[Fe(CN)]_6$ has a strong effect on the morphology of the resultant products. In Fig. 1a, $K_3[Fe(CN)]_6$ concentration was 15 mM, the morphology appeared square sheet about 20 nm, AuNPs was around 1–3 nm (Fig. 1a and b), The corresponding EDS spectrum of nanocomposites shows the peaks presence of C, N, K, Au and Fe elements (insert in Fig. 1b). When increasing the concentration to 20 mM, PPy/PB shell presented compact network, AuNPs were uniform distributed in PPy/PB shell and the size was around 2–3 nm. As the concentration reached to 25 mM, such compact-network PPy/PB shell appeared again, but rodlike AuNPs appeared and recessed irregularly into PPy/PB shell, it is about 2 nm width and 40 nm length (Fig. 1d).

15 mM $K_3[Fe(CN)]_6$ is a optimization concentration and has been chosen to do the subsequent experiment. Nevertheless, it is difficult to distinguish PPy and PB around AuNPs, there may be two reasons: the color of PB in the TEM image is light, the other is that PB embraced by PPy fully, which is favourable to avoid the PB leaking and improve the catalysis of PB.

Actually, with the addition of pyrrole monomers into mixture solution, the autopolymerization of pyrrole into PPy and $AuCl_4^-$ was reduced to elemental Au instantaneously and simultaneously (Eq. (1)) [43]. At the same time, PB produced along with elemental Au. The forming of PB involves the reduction of the free ferric ion or the ferric ion in the associated complex, according to Eq. (3), elemental Au acts as a catalyst in this progress [46–48]. This reaction is unfavourable thermodynamically because the standard free-energy change is 173 kJ mol^{-1}. The driving force could be provided only by the subsequent formation of PB (Eq. (2)). The standard free-energy change of the total reaction is −177 kJ mol^{-1}. The reaction mechanisms may be as follows:

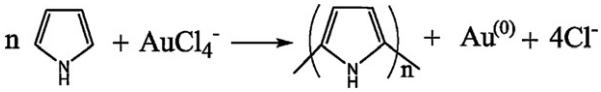

(1)

$$K^+ + Fe^{2+}Fe(CN)_6^{3+} \rightarrow KFe^{3+}[Fe^{2+}(CN)_6] \quad (2)$$

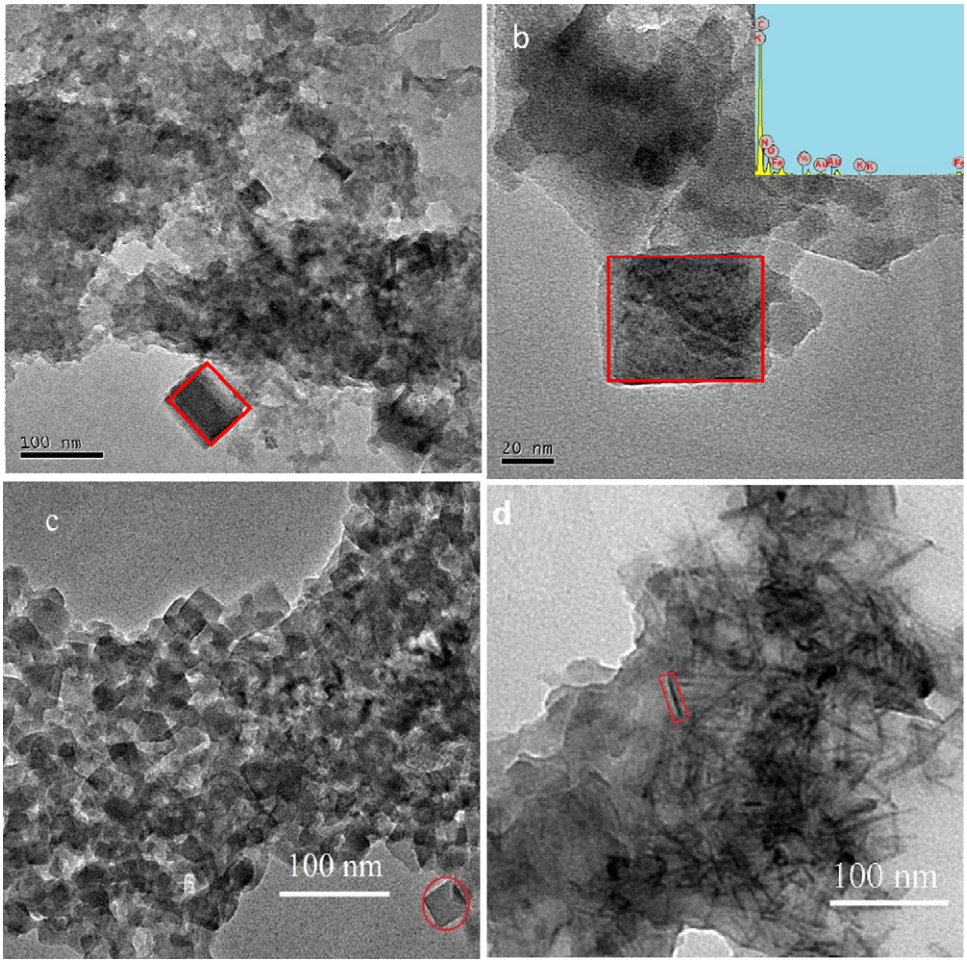

Fig. 1. TEM images of Au–PPy/PB core–shell nanocomposites at different $K_3[Fe(CN)]_6$ concentrations: (a) 0.5 mM, (b) 5 mM, (c and d) 15 mM, (f) 25 mM, and (g) 30 mM. Synthetic conditions: pyrrole 0.1 M; $HAuCl_4$ 1 mM; reaction time 2 h; room temperature. EDS of Au–PPy/PB core–shell nanocomposites at 15 mM $K_3[Fe(CN)]_6$ concentrations (e).

$$Fe^{3+} + \frac{1}{2}H_2O \rightarrow \frac{1}{4}O_2 + H^+ + Fe^{2+} \quad (3)$$

The molecular structure of the Au core–PPy/PB shell structured nanocomposites was characterized by XRD pattern, as shown in Fig. 2a. The broad peak with 2θ at 24.50° is related to the diffraction of PPy which is the characteristic of the disordered PPy structured features [49,50], and the other peaks with 2θ at 17.28°, 24.64°, 35.16°, 39.50°, 50.75° are related to 100, 110, 200, 210, 220 diffraction of PB, respectively [51]. Besides, the peaks at 44.42°, 64.72° are corresponding to the diffraction of Au(2 0 0), Au(2 2 0).

Fig. 2b shows the FTIR spectra of Au–PPy nanocomposites (i) and Au–PPy/PB core–shell nanocomposites (ii). The characteristic PPy peaks are located at 1540 and 1458 cm^{-1}, due to the pyrrole ring stretching and conjugated C–N stretching mode, respectively [52,53]. However, the band is very weak, which might be the polymerization degree of PPy is low, or the lack of observation caused by other strong absorptions. The peaks at 1043 cm^{-1} is related to the in-plane vibrations of =C–H and 750 cm^{-1} is attributable to C–H wagging vibration [54]. The presence of band at 3444 cm^{-1} corresponds to N–H stretching vibration. These spectral features indicate that pyrrole polymerize into PPy perfectly in the one-step progress. A strong absorption band at 2079 cm^{-1} shows the common characteristics of PB, corresponding to the stretching vibration of the CN group [55], and the band at 503 cm^{-1} is assignable to M–CN–M′, which indicates the presence of PB. In the IR spectrum of Au–PPy, the characteristic peak of PPy is much clear. Compared Au–PPy with Au–PPy/PB IR data, it can be seen that PB is formed at the catalysis of Au(0) in the one-step progress.

To get more informations of the composition, UV–vis absorption spectra of Au–PPy/PB nanocomposites was shown in Fig. 2c. Because AuNPs and PB, PPy show absorption in the UV–vis region, the spectrum for the nanocomposites was recorded in the region 400–800 nm. The band at 460 nm is attributable to the π–π^* transition of PPy chains which is well consistent with the reported data in Fig. 2c [42]. The absorption of PB is at 700 nm, which is due to the mixed-valence charge-transfer absorption of the polymeric Fe(II)–CN–Fe(III) [56]. At the same time, we can observe the surface plasmon band of Au nanoparticles is at 550 nm [29], which is shifted to longer wavelengths in comparison to Au colloid solution that is synthesized by citrate (inset), owing to AuNPs has a strong interaction with PB. The peak is weak, but it has not been covered by PPy and PB broad absorption, which indicates that AuNPs could be surrounded by PPy matrix and PB efficiently.

3.2. Electrochemical behavior of Au–PPy/PB core–shell nanocomposites modified GCE

To investigate the electrochemical property, cyclic voltammograms (CVs) was used. Fig. 3a shows the CVs of the modified GCE in 0.02 M PBS + 0.1 M KCl (pH = 3) at a scan rate of 50 mV s^{-1}: (i) in the absence of H_2O_2 and (ii) in the presence of 1.0×10^{-8} M H_2O_2. In

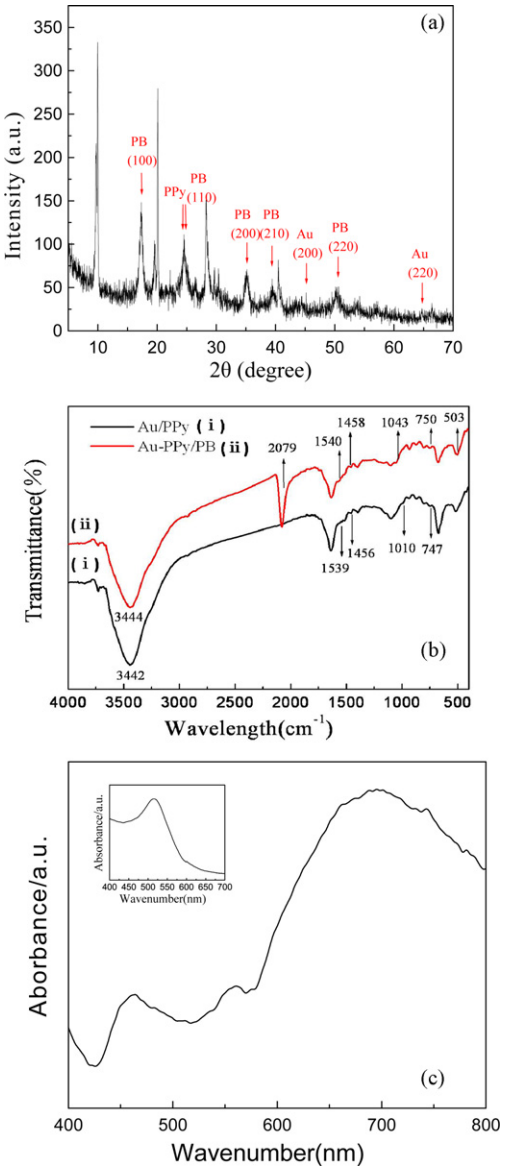

Fig. 2. (a) XRD pattern of Au–PPy/PB core–shell nanocomposites. (b) FTIR spectrum of Au–PPy/PB core–shell nanocomposites and Au–PPy nanocomposites. (c) UV–vis absorption spectra of Au–PPy/PB core–shell nanocomposites. Inserted is the UV–vis absorption spectra of AuNPs.

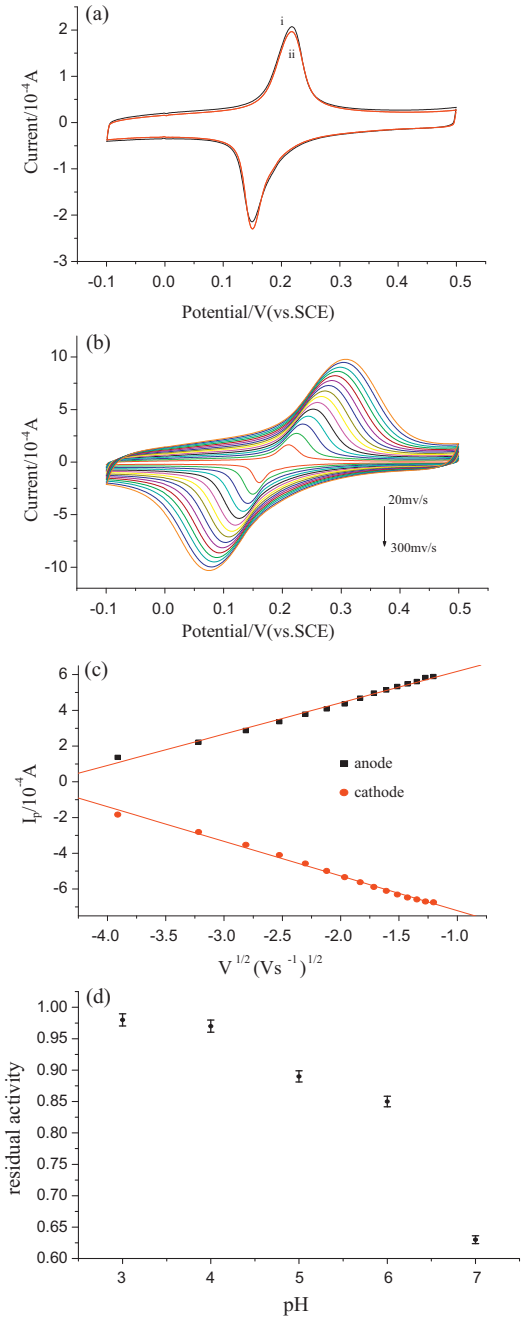

Fig. 3. (a) CVs of a Au–PPy/PB core–shell nanocomposites modified electrode in 0.02 M PBS + 0.1 M KCl (pH = 3), at a scan rate of 50 mV s^{-1}: (i) in the absence of H_2O_2 and (ii) in the presence of 1.0×10^{-8} M H_2O_2. (b) CVs of a Au–PPy/PB core–shell nanocomposites modified GCE in 0.02 M PBS + 0.1 M KCl (pH = 3) on scan rates 20, 40, 60, 80, 100, 120, 140, 160, 180, 200, 220, 240, 260, 280 and 300 mV s^{-1}. (c) Dependence of peak currents on scan rates. (d) CVs peak currents of Au–PPy/PB core–shell nanocomposites modified GCE dependent on pH in 0.02 M PBS + 0.1 M KCl.

the absence of H_2O_2, the modified electrode gives no response and only a reversible electrochemical response of PB can be observed. It is well-known that Prussian white, its reduced form, is capable of catalyzing reduction of H_2O_2 at low potentials. When added to 1.0×10^{-8} M H_2O_2, the CVs curve changes with a decrease of the oxidation current and a simultaneous increase of the reduction current. It indicates that the H_2O_2 produced electrocatalytic reduction is preferable for H_2O_2 detection.

The effect of the potential scanning rate (v) on the peak current was studied in the range of 20–300 mV s^{-1}, which is used to evaluate the kinetics of the modified electrodes, as shown in Fig. 3b. With the increase of scanning rate, the anodic peak potential shifts to a more positive direction and the cathodic peak potential shifts to a more negative direction. The influence of v on the redox peak currents (I_p) is shown in Fig. 3c. I_p has a linear relationship with $v^{1/2}$, and the regression equation is I_{pa} (10^{-4} A) = 7.933 + 1.7539 $v^{1/2}$ (r = 0.9960), indicating a diffusion controlled process of PB on the electrode. The electrochemical parameters could be calculated using the formula by Laviron [57]:

$$\log K_s = a \log(1-a) + (1-a) \log a - \log\left(\frac{RT}{nFv}\right) - a(1-a)nF\frac{\Delta E_p}{2.3RT}$$

where α is the electron transfer coefficient, n is the electron transfer number, K_s is the apparent electron transfer rate constant, R is the gas constant, T is the absolute temperature, and ΔE_p is the peak-to-peak separation. The values of a and K_s are 0.5 and 2.25 s^{-1},

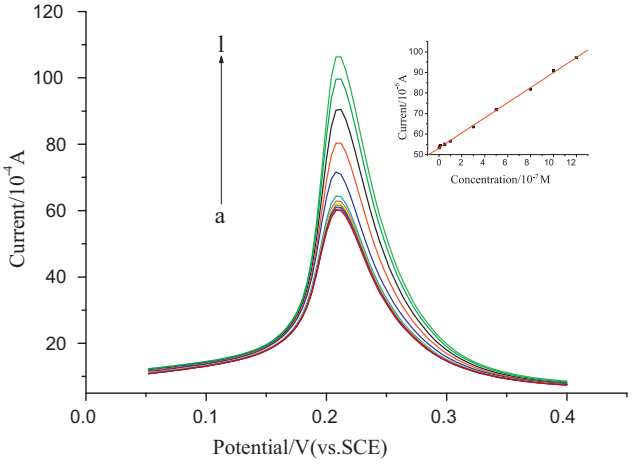

Fig. 4. DPV curves of Au–PPy/PB core–shell nanocomposites modified electrode in 0.02 M PBS + 0.1 M KCl (pH = 3), at a scan rate of 50 mV s^{-1}. (a) blank; (b) 1.0×10^{-9} M; (c) 2.5×10^{-9} M; (d) 5.0×10^{-9} M; (e) 1×10^{-8} M; (f) 5.0×10^{-8} M; (g) 1.0×10^{-7}M; (h) 3.0×10^{-7} M; (i) 5.0×10^{-7} M; (j) 8×10^{-7} M; (k) 1.0×10^{-6} M; (l) 1.2×10^{-6} M.

respectively. The calculated results reveal that AuNPs and PPy have the synergistic effect as to enhance the electrochemical reaction rate constant of PB on the electrode.

3.3. The pH stability of Au–PPy/PB core–shell nanocomposites modified GCE

Investigation of the effect of the pH value on the performance of the biosensor is of great importance, because the main disadvantage of the PB based sensing layers in respect to long-term continuous monitoring is their inherent instability, particularly in neutral solutions. Typical experiments methods to evaluate the stability of PB calculate the decreased value of the peak currents using the CV. 100 cycles of CV were performed between −0.1 and 0.5 V at a scan rate of 50 mV s^{-1} in pure base electrolyte solution under different pH conditions, the residual activity was obtained by calculating the ratio of the peak current of the end cycle to the first cycle, as shown in Fig. 3d. When pH is 3.0 and 6.0, the current of the modified GCE dropped 2% and 15%, respectively. The results shows that integrating both conducting polymers and metal nanoparticles have great effects to improve the electrochemical stability of the PB: AuNPs in nanocomposites can increase the surface dimension and provide a better loading capacity for the PB. Besides, PPy, which has the unique structure-matrix, can cover PB perfectly and protect PB in nanocomposites from leaking to a certain degree, thus enhance the stability of PB in long-term continuous monitoring. At pH 3 in buffer solution, the modified GCE is most stable and was used in next experiment.

3.4. Electrocatalytic activity of Au–PPy/PB core–shell nanocomposites modified GCE toward H_2O_2

Au–PPy/PB core–shell nanocomposites were immobilized onto the surface of a GCE and the modified GCE was made, which was used to determine different concentrations of H_2O_2 under the optimum conditions, DPV curves are shown in Fig. 4. The linear relationship has been established between the oxidation peak current and the concentration of H_2O_2. The range is from 2.5×10^{-9} to 1.2×10^{-6} M with a correlation coefficient of 0.9990, and the detection limit reaches to 8.3×10^{-10} M H_2O_2. In terms of the improved detection limit, two main factors are taken into account, one is that AuNPs and PPy can provide low ohmic drops resulting in the rate constant of the electron transfer process enhancing, the other is that much higher surface area of PPy matrix give sites for PB and AuNPs loading effectively and reduce the leakage unnecessarily under the long-term continuous detection.

3.5. The reproducibility and stability of the biosensor

In this work, the reproducibility and the stability of the biosensor was evaluated by measuring the amperometric response at 1.0 mM H_2O_2. The reproducibility was evaluated for five identical electrodes prepared independently in different days following the same experimental protocol and the results revealed that the biosensor has satisfied reproducibility with a relative standard deviation (RSD) of 5.2%. The long-term stability of the biosensor was evaluated by measuring the sensitivity of the biosensor to addition of 1.0 mM H_2O_2 at 3 days interval. Between measurements, the biosensor was stored at 4 °C. Compared with its initial activity, the response sensitivity maintained 95% after 30 days.

4. Conclusions

We have presented a one-step method for the synthesis of multi-component nanocomposites in water solution at room temperature. Then Au–PPy/PB nanocomposites were immobilized on the GCE and construct a H_2O_2 biosensor. The biosensor exhibited high sensitivity, fast response and non-interferences. The method is green, easily scalable and available and can be extended to prepare other multi-component nanocomposites used for catalyst and other applications.

Acknowledgements

This work was supported by the National Natural Science Foundation of China (Nos. 20927004, 21005063, and 21175108), the Science and Technology Support Projects of Gansu Province (No. 090GKCA036), and Key Laboratory of Polymer Materials of Gansu Province, China.

References

[1] J.A. Asecencio, M.L.J. Guo, X. Cheng, C.F. Chou, Nano Letters 4 (2004) 69–73.
[2] R. Gangopadhyay, A. De, Chemistry of Materials 12 (2000) 608–621.
[3] P. Innocenzi, G. Brusatin, Chemistry of Materials 13 (2001) 3126–3139.
[4] H. Kim, A.A. Abdala, C.W. Macosko, Macromolecules 43 (2010) 6515–6530.
[5] J. Zheng, Z. Zhu, H. Chen, Z. Liu, Langmuir 16 (2000) 4409–4412.
[6] Y. Mizukoshi, K. Okitsu, Y. Maeda, T.A. Yamamoto, R. Oshima, Y.J. Nagata, Journal of Physical Chemistry B 101 (1997) 7033–7037.
[7] S.I. Dolgaev, A.V. Simakin, V.V. Voronov, G.A. Shafeev, F.B. Verduraz, Applied Surface Science 186 (2002) 546–551.
[8] A. Henglein, D. Meisel, Langmuir 14 (1998) 7392–7396.
[9] M.C. Bourg, A. Badia, R.B. Lennox, Journal of Physical Chemistry B 104 (2000) 6562–6567.
[10] G. Peto, G.L. Molnar, Z. Paszti, O. Geszti, A. Beck, L. Guczi, Materials Science and Engineering C 19 (2002) 95–99.
[11] S.H. Tsai, Y.H. Liu, P.L. Wu, C.S. Yeh, Journal of Materials Chemistry 13 (2003) 978–980.
[12] C. Perruchot, M.M. Chehimi, D. Mordenti, M. Brianda, M. Delamara, Journal of Materials Chemistry 8 (1998) 2185–2193.
[13] Z.H. Han, H.Y. Zhu, S.R. Bulcock, S.P. Ringer, Journal of Physical Chemistry B 109 (2005) 2673–2678.
[14] R.Y. Zhang, X.M. Wang, Chemistry of Materials 19 (2007) 976–978.
[15] J.B. Di, D.Y. Sogah, Macromolecules 39 (2006) 5052–5057.
[16] K. Mallick, M.J. Witcomb, R. Erasmus, M.S. Scurrell, Materials Science and Engineering B 140 (2007) 66–171.
[17] Q.L. Tang, K.W. Wang, Y.J. Zhu, F. Chen, Materials Letters 63 (2009) 1332–1334.
[18] S.S. Kumar, J. Joseph, K.L. Phani, Chemistry of Materials 19 (2007) 4726–4730.
[19] B.T.T. Nguyen, J.Q. Ang, C.S. Toh, Electrochemistry Communications 11 (2009) 1861–1864.
[20] A.K.M. Kafi, F. Yin, H.K. Shin, Y.S. Kwon, Current Applied Physics 7 (2007) 496–499.
[21] T.H. Kuo, C.Y. Hsu, K.M. Lee, K.C. Ho, Solar Energy Materials and Solar Cells 93 (2009) 1755–1760.
[22] A.J. Eftekhari, Power Sources 126 (2004) 221–228.
[23] L.C. Chen, Y.H. Huang, K.S. Tseng, K.C.J. Ho, Journal of New Materials for Electrochemical Systems 5 (2002) 203–212.
[24] D.M. Cheng, H.B. Xia, H.S.O. Chan, Langmuir 20 (2004) 9909–9912.

[25] Y.C. Liu, H.T. Lee, S.J. Yang, Electrochimica Acta 51 (2006) 3441–3445.
[26] H. Liu, Z. Shi, J. Zhang, L. Zhang, Journal of Materials Chemistry 19 (2009) 370–374.
[27] X.X. Yuan, X. Zeng, H.J. Zhang, Z.F. Ma, C.Y. Wang, Journal of the American Chemical Society 132 (2010) 1754–1755.
[28] H. Dong, X.D. Cao, C.M. Li, ACS Applied Materials & Interfaces 1 (2009) 1599–1606.
[29] K. Zeng, H. Tachikawa, Z.Y. Zhu, V.L. Davidson, Analytical Chemistry 72 (2000) 2211–2215.
[30] H. Yoon, S. Ko, J. Jang, Journal of Physical Chemistry B 112 (2008) 9992–9997.
[31] W. Chen, Z.S. Lu, C.M. Li, Analytical Chemistry 80 (2008) 8485–8492.
[32] Y.H. Huang, J.B. Goodenough, Chemistry of Materials 20 (2008) 7237–7241.
[33] J. Wang, C.O. Too, D. Zhou, G.G. Wallace, Journal of Power Sources 140 (2005) 162–167.
[34] L.W. Ji, Y.F. Yao, O. Toprakci, Z. Lin, Y.Z. Liang, Q. Shi, A.J. Medford, Journal of Power Sources 195 (2010) 2050–2056.
[35] B.C. Kim, J.M. Ko, G.G. Wallace, Journal of Power Sources 177 (2008) 665–668.
[36] S.R. Sivakkumar, J.M. Ko, D.Y. Kim, B.C. Kim, G.G. Wallace, Electrochimica Acta 52 (2007) 7377–7385.
[37] J.H. Kim, A.K. Sharma, Y.S. Lee, Materials Letters 60 (2006) 1697–1701.
[38] E. Hermelin, J. Petitjean, J.C. Lacroix, K.I. Chane-Ching, J. Tanguy, P.C. Lacaze, Materials Letters 20 (2008) 4447–4456.
[39] D.E. Tallman, K.L. Levine, C. Siripirom, V.G. Gelling, G.P. Bierwagen, S.G. Croll, Applied Surface Science 254 (2008) 5452–5459.
[40] D.O. Flamini, S.B. Saidman, Corrosion Science 52 (2010) 229–234.
[41] J. Njagi, S. Andreescu, Biosensors and Bioelectronics 23 (2007) 68–175.
[42] S.T. Selvan, J.P. Spatz, H. Klok, M. Moller, Advanced Materials 10 (1998) 32–134.
[43] Y.C. Liu, T.C. Chuang, Journal of Physical Chemistry B 107 (2003) 12383–12386.
[44] C.R.K. Rao, D.C. Trivedi, Synthetic Metals 157 (2007) 432–436.
[45] X.Q. Lu, J. Du, Journal of Physical Chemistry C 114 (2010) 14786–14793.
[46] J.D. Qiu, H.Z. Peng, R.P. Liang, J. Li, X.H. Xia, Langmuir 23 (2007) 2133–2137.
[47] D. Ellls, M. Eckhoff, V.D. Neff, Journal of Physical Chemistry 85 (1981) 1225–1231.
[48] K. Itaya, I. Uchida, Inorganic Chemistry 25 (1986) 389–392.
[49] Y. Kojima, A.A. Usuki, M. Kawasumi, A. Okada, T. Kurauchi, O. Kamigaito, Journal of Polymer Science A: Polymer Chemistry 31 (1993) 983–986.
[50] I. Seo, M. Pyo, G. Cho, Langmuir 18 (2002) 7253–7257.
[51] S.Q. Liu, J.J. Xu, H.Y. Chen, Electrochemistry Communications 4 (2002) 421–425.
[52] G. Cho, B.M. Fung, D.T. Glatzhofer, J.S. Lee, Y.G. Shul, Langmuir 17 (2001) 456–461.
[53] J. Jang, J.H. Oh, Advanced Functional Materials 15 (2005) 494–502.
[54] G.I. Mathis, V.T. Troung, Synthetic Metals 89 (1997) 103–109.
[55] J.B. Ayers, W.H. Piggs, Journal of Inorganic and Nuclear Chemistry 33 (1971) 721–733.
[56] K. Itaya, I. Uchida, V.D. Neff, Accounts of Chemical Research 19 (1986) 162–168.
[57] E. Laviron, Journal of Electroanalytical Chemistry 101 (1979) 19–28.